Chronological Molecular Fingerprint of Wetland Soil by Sensitivity-Enhanced Solid-State NMR

Wancheng Zhao[1,#], Elizabeth C Thomas[2,#], Debkumar Debnath[1], Faith Scott[3], Frederic Mentink-Vigier[3], John R. White[4], Robert L. Cook[2,*], Tuo Wang[1,*]

[1] Department of Chemistry, Michigan State University, East Lansing, MI 48824, USA

[2] Department of Chemistry, Louisiana State University, Baton Rouge, LA 70803, USA

[3] National High Magnetic Field Laboratory, Tallahassee, FL 23310, USA

[4] Department of Oceanography & Coastal Sciences, Louisiana State University, Baton Rouge, LA 70803, USA

[#]These authors contributed equally to this work.

*Correspondence: wangtuo1@msu.edu; rlcook@lsu.edu

This manuscript file contains:

Main text with figures embedded, Methods, References, and Extended Data Figures

Abstract

Soil organic matter (SOM) plays a major role in mitigating greenhouse gas emission and thereby regulating Earth's climate, carbon and water cycles, and biodiversity. Wetland soils contain the highest stores of soil carbon on the planet on an areal basis, accounting for one-third of all the SOM, yet our understanding of carbon sequestration within wetlands lags behind that of upland soils. Here we show the molecular-level fingerprints of wetland soils spanning eleven centuries using advanced solid-state nuclear magnetic resonance (ssNMR) spectroscopy. Remarkably, combining dynamic nuclear polarization (DNP) with SOM enrichment allowed up to an 8,000-fold time-saving over conventional NMR approaches. This innovative approach for SOM characterization revealed that the parent herbaceous plant core molecular structures are preserved, with the aromatic and carbohydrate motifs becoming tightly packed, even after a millennium. Such preserved cores occur alongside molecules from the decomposition of loosely packed parent biopolymers and biogeochemical processing driven by geological global and anthropogenic changes, adding to the chemical diversity of SOM. These findings reveal that particulate organic matter (POM) should be a major focus for wetlands, and other soils with high organic matter content, especially when considering the fate of coastal wetland SOM when exposed to oxygenated water due to erosion.

Main

Soil organic matter (SOM) and associated soil organic carbon (SOC), critically represents one of the major reservoirs of carbon on the planet and is critical to ecosystem services, from the molecular to the global scale[1,2]. Just the top 1 m of the world's soil contains 1500 petagrams (Pg, billion tons) of carbon, approximately twice the carbon pool contained in the entire atmosphere[3] and more than the atmosphere and vegetation combined[4]. Soil has been a sink to about 210 ± 45 Pg of carbon between the years 1850 and 2021, mitigating around 100 ppm of atmospheric CO_2 levels[5]. Wetland soils contain approximately one-third of this SOC despite occupying only 5-6% of the Earth's land surface area[6]. Coastal wetlands, known as the blue carbon ecosystems, occupy only 0.07-0.22% of the Earth's surface but sequester 0.08-0.22 Pg carbon each year, accounting for more than half of the carbon buried in the oceans annually[7-9], and store the vast majority of this carbon for hundreds to thousands of years, with minimal methane emissions due to a poised redox potential[10].

The anaerobic conditions of wetland soil cause a reduced metabolic efficiency of microbes in acquiring energy during decomposition of complex organic carbon compounds, which leads to increased preservation of carbon in soil profile unless hydrologic conditions change[11]. Subsidence, sea level rise and wave energy promote wetland soil collapse into the surrounding shallow, estuarine aerobic water column, resulting in the oxidation of SOM and releasing the stored carbon back to the atmosphere as primarily carbon dioxide[12-14]. To preserve and manage wetlands, minimize greenhouse gas emissions, and maximize carbon sequestration potential, it is crucial to understand, model, and accurately predict the dynamics of SOM, and hence SOC, in a scalable and applicable manner[15]. Thus, detailed molecular information, including functionality, isomerism, and conformations of the sequestered carbon pool is a fundamental requirement. Currently, there is limited work on this advanced level of carbon sequestration within coastal wetlands, as most work has been focused on upland soils.

The persistence of SOC was considered to occur through the formation of recalcitrant macromolecules by polymerization during a process called humification[16]. Presently, the dynamic stability concept prevails, whereby organic carbon is preserved as an organic entity via molecular preservation for periods of time, in concert with dynamically changing organic carbon speciation[17]. This new view also breaks SOM down into two major pools: particulate organic matter (POM), which includes occluded SOM and plant materials, and mineral associated organic matter (MAOM), which contains mostly small organic molecules and biological metabolites[18,19]. Over time, these two more recalcitrant pools may become accessible, and therefore can be viewed as shorter-term stable carbon deposits in the context of geologic time[20] (Swift and Hayes, 2020). Most research on this new paradigm was focused on upland or mineral soils, with the MAOM fraction receiving the bulk of the attention, although the focus is beginning to shift[19,21,22]. Most coastal wetlands are POM-dominated systems with a high organic matter to mineral matter ratio. Globally, per unit area, coastal wetlands are considered the most carbon-rich dynamic reservoirs of organic carbon, warranting a closer examination of this critical and most vulnerable to loss carbon pool, as sea level continues to rise.

Here, we examine coastal wetland soil samples from the Mississippi River Delta, USA that have been deposited and preserved over the past 11 centuries, but whose soil C stores are being lost at

an accelerated rate due to the high relative sea level rise rate. Sensitivity-enhanced ssNMR is applied, for the first time, to whole soil samples to enable rapid acquisition of 2D $^{13}C/^{1}H$-^{13}C correlation spectra, providing atomic-level structural information of the carbon fraction of SOC. This method allows for a detailed characterization of soil on the fine granular and molecular level, beyond the moiety characterization level (**Supplementary Discussion**), which reveals that: 1) in the initial stages of SOC sequestration, core structures of the parent herbaceous plant materials are preserved but the aromatic and carbohydrates motifs become tightly packed, with non-carbohydrate components being concentrated in the soil, 2) some structural cores of herbaceous plant biopolymers survive anaerobic microbial degradation, with their original structure and physical packing preserved up to 1000 years since deposition, 3) molecules from the decomposition of loosely packed parent biopolymers and biogeochemical processing are present and add to the diversity of SOC chemical nature, and 4) changes in the carbon speciation during the sequestration processes are driven by both natural geological changes (e.g., delta lobe switching) as well as anthropogenic changes (e.g., river levees). Besides these multifaceted conceptual advances, this high-resolution and rapid technological platform also opens a new research avenue for SOC analysis in undisturbed soil materials.

Results

Molecular Fingerprinting of carbohydrate and aromatics in wetland soil

We examined seven soil samples (down to almost 2 m) collected from a salt marsh *Spartina alterniflora*-vegetated island in the Barataria Bay, Louisiana, located along the Gulf of Mexico coastline (**Extended Data Fig. 1a-d**). Each year, Louisiana experiences a loss of over 65 km^2 of coastal wetlands, leading to an annual release of over 1 million metric tons of stored carbon from Barataria Basin alone[23,24]. This island underwent shoreline erosion rates of over 1.5 m y^{-1} and became entirely eroded in 2021 (**Extended Data Fig. 1e, f**). A two-step protocol was developed to improve the NMR sensitivity by a factor of 90, reducing experimental duration 8,100 times, essentially reducing a 22-year-long experiment down to one day. This was achieved by employing hydrofluoric acid (HF) treatment, which depleted the mineral component, concentrated SOM, and enhanced their signals by a factor of 5 (**Fig. 1a**) without chemically perturbing its structure as described in **Supplementary Methods**[25-27], and DNP, which relies on microwave irradiation to transfer electron polarization to NMR-active nuclei in the soil, resulting in an additional 18

enhancement (**Fig. 1b**). Together, this allowed for carbon connectivity to be directly mapped by a 2D ^{13}C-^{13}C correlation spectrum on unlabeled soil (**Fig. 1c**), a task previously impossible by conventional techniques, but now achievable within 16 hours of analytical time.

The carbohydrate signals of the top 10-cm layer of soil (sample 1) were predominantly from cellulose (**Fig. 1c**), including the glucan chains residing on both the surface and internal domains of the microfibrils (**Fig. 1d**). Multiple forms of glucan chains are identifiable within cellulose. First, we observed two distinct sets of signals from surface chains (s^f and s^g in **Fig. 1c**), which have been proposed to contribute to distinctly hydrated exteriors of the microfibrils, namely the concept of hydrophobic and hydrophilic surfaces[28]. Second, in addition to the dominant interior conformers (i^a and i^b), a third form of i^c was also identified in a 2D ^{1}H-^{13}C correlation spectrum, collected within an hour (**Fig. 1e**), with a unique C4 chemical shift of 87.5 ppm. Type-c glucan has been found in the native cellulose across many different grass and woody plant species and have been attributed to the deeply embedded and inaccessible core of the larger bundle formed by multiple microfibrils (**Fig. 1d**)[29-31]. The identification of these five glucan types demonstrates that the native cellulosic material has been preserved in surface soil.

Further structural preservation is indicated by the unexpected identification of 2-fold and 3-fold xylan (Xn^{2f} and Xn^{3f}) in the soil (inset of **Fig. 1c**). The 2-fold and 3-fold refers to the helical screw conformation and indicate the number of sugar residues needed for finishing a 360° helical rotation along the chain (**Fig. 1f**)[32]. Recent studies of the lignocellulosic plant biomass have revealed the distinct functions of these two xylan conformers, with the flat-ribbon 2-fold xylan coating the smooth surface of cellulose microfibrils[33,34] and the zigzag 3-fold xylan preferentially packing with disordered aromatics, namely the lignin domains in plants[30]. Evidently, at least a portion of the structural core of plant lignocellulosic biomass is preserved, intact, in the wetland soil.

Many non-carbohydrate molecules were also identified, including the aromatics and methoxy substitutions in lignin, the acyl chains (or polymethylene[35]) in lipid polymers, and other aliphatic motifs (**Fig. 1e**). This characterization was achieved using a single-hour 2D experiment that relies on a short CP contact time (0.1 ms) to emphasize one-bond ^{1}H-^{13}C correlations. Protonated carbons in lignin exhibited signals in the ^{13}C chemical shift range of 110-125 ppm (blue spectrum in **Fig.**

1g). The 105 ppm ^{13}C signals have dual contributions from both carbohydrates and aromatics, including the carbon 1 of cellulose and 2-fold xylan, as well as the carbons 2 and 6 of the S-unit, thus showing one-bond correlations with both carbohydrate and aromatic protons.

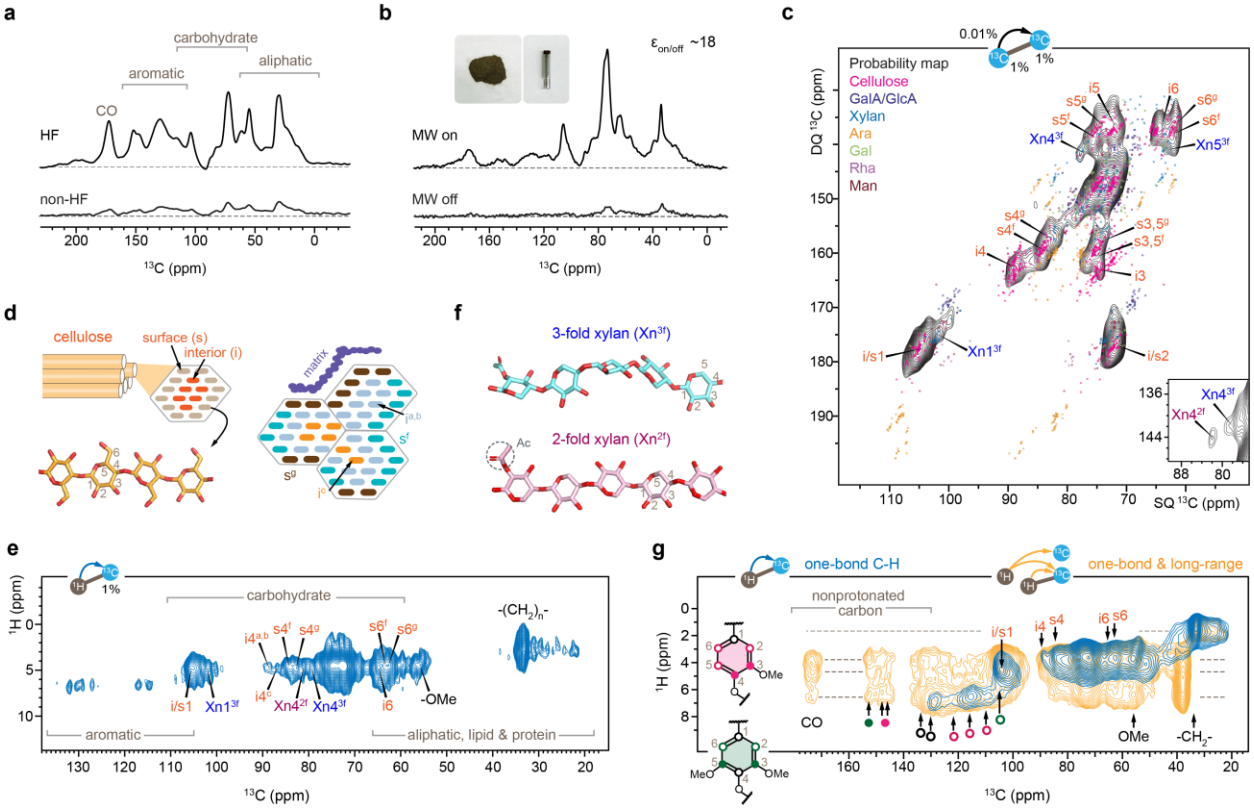

Fig. 1 | Molecular fingerprint and spatial organization of biopolymers in wetland soil. a, Comparison of quantitative ^{13}C spectra of the HF and non-HF treated soil sample 1 (surface layer) at room temperature. HF treatment concentrates the organic phase and gives a 5-fold sensitivity boost. **b,** Comparison of 1D ^{13}C spectra with and without microwave (MW) irradiation. The sensitivity enhancement ($\varepsilon_{on/off}$) provided by DNP is 18-fold. Inset shows pictures of the soil sample and a sapphire rotor containing the soil sample. **c**, DNP-enabled 2D ^{13}C-^{13}C correlation spectrum (refocused J-INADEQUATE) of soil sample 1 measured in 16 h, resolving the carbon connectivity of carbohydrate components. Overlay of the measured spectrum (black) with the probability map constructed using 412 carbohydrate units from Complex Carbohydrate Magnetic Resonance Database[36] indicates the best match with cellulose (magenta dots). Assignments of the interior (i) and surface (s) glucan chains of cellulose microfibrils and the xylose units of 2- and 3-fold xylans (Xn^{2f} and Xn^{3f}) are labeled. Inset shows the xylose carbon 4 region processed with large line-broadening to show xylan signals. **d**, Representative cellulose structure with each microfibril containing eighteen β-1,4-glucan chains on the surface and interior domains. Multiple microfibrils aggregate to form larger bundles that accommodate different forms of glucan chains ($i^{a,b}$, i^c, s^f, and s^g), which are further wrapped by matrix non-cellulosic polymers. **e**, Single-hour DNP 2D ^1H-^{13}C correlation spectrum resolves the signals from aliphatic carbons, carbohydrates, and aromatics. Key signals of polymethylene ($-CH_2-)_n$, methoxyl ($-OCH_3$), cellulose, and xylan are labeled. **f**, Structure of 2- and 3-fold xylan conformers. **g**, Overlay of 2D ^1H-^{13}C correlation spectrum measured with short (0.1 ms; blue) and long (1.0 ms; yellow) CP contact times.

The symbolic representations correspond to the carbons in lignin monolignol units. Dashed lines show the key ^{1}H positions.

A range of nonprotonated carbons were also observed with a longer CP contact (1.0 ms) that extended the reach of ^{1}H-^{13}C correlation (yellow spectrum of **Fig. 1g**; **Extended Data Fig. 2**). The spotted signals included carbonyl groups (CO) and monolignols, such as the carbon 3 and 5 of the syringyl (S) unit at 154 ppm and the carbon 3 and 4 of the guaiacyl (G) unit at 145-149 ppm. Their chemical nature was confirmed by their strong peaks in dipolar-dephasing spectra that removed all protonated carbon signals (**Extended Data Fig. 3**). The NMR observations of SOC unveiled a complex composition in terms of plant polysaccharides, lignin, and lipid polymers.

Domain distribution of polymers in soil

It is noticeable that the aromatic carbons (^{13}C chemical shifts of 100-140 ppm) not only show cross peaks with the aromatic protons at 6-7 ppm, but also cross-talked with carbohydrate and aliphatic protons that resonate at 3-5 ppm, revealing the co-localization of aromatics, aliphatics, and carbohydrates on the nanoscale, consistent with previous work[37]. This concept of molecular mixing is also supported by the cross peaks between carbohydrate carbon sites (^{13}C chemical shifts of 70-110 ppm) with aromatic protons (^{1}H chemical shifts of 6-7 ppm). The only exception was observed in polymethylene (-CH_2-), which failed to show correlations with other carbons or protons, providing a clear indication of domain separation for lipid polymers. This finding corroborates earlier ssNMR results[35,37] where poly-methylene were found to form large aggregates to resist further degradation, which is a characteristic commonly shared by diverse soil materials in nature.

Preserved structural core in plant material and surface soil

The composition of plant detritus inputs to the soil as well as the redox status of the soil are among the key external factors that affect the rate of carbon sequestration[38]. The plant tissues gathered at the soil collection site retain highly similar carbohydrate signals when compared to the surface soil (**Fig. 2a**). Cellulose crystallinity is unchanged, as evidenced by both soil and plant samples showing comparable intensity ratios between the interior cellulose C4 at 89 ppm and the surface cellulose C4 at 84 ppm. With a 24-fold DNP enhancement (**Extended Data Fig. 4**), we unambiguously detected the varied signals from multiple cellulose forms and xylan conformers in

2D ^{13}C-^{13}C correlation spectrum of these plants (**Fig. 2b**), which demonstrated a similar pattern to the soil spectrum. The soil exhibits elevated levels of carbonyls, methoxyls, aromatics, and aliphatics, as revealed by the difference of two parental spectra (**Fig. 2a**). These components might have accumulated due to their slower decomposition rate when compared to carbohydrates.

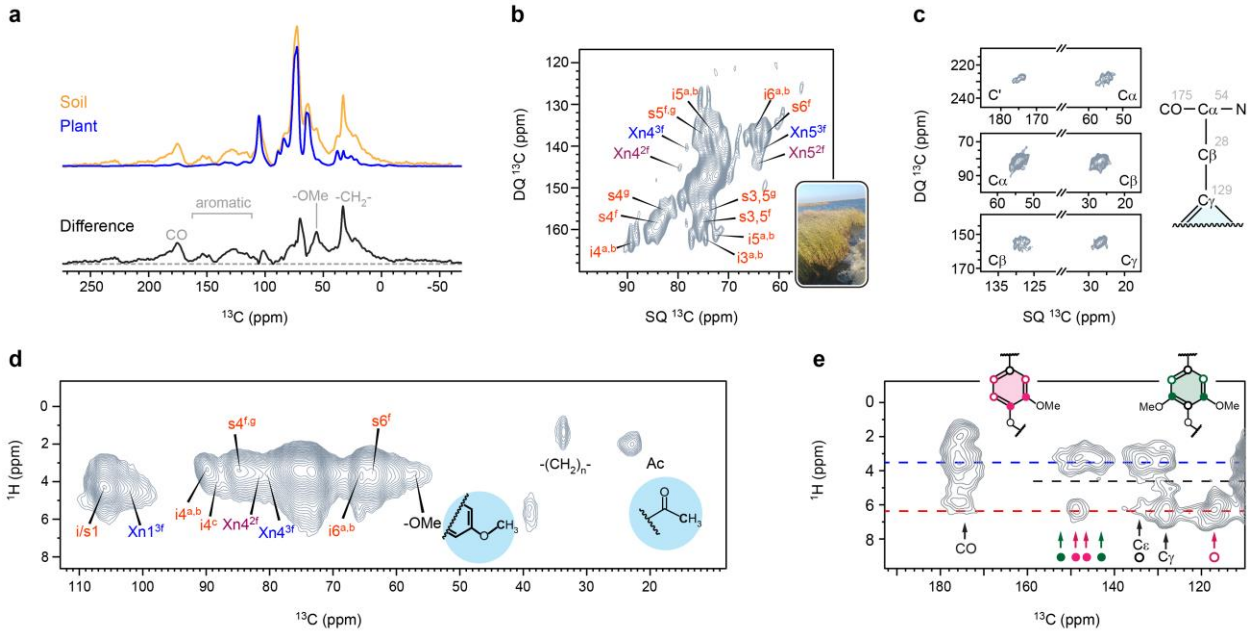

Fig. 2 | Conserved structural core of plant material and wetland soil. a, DNP-enhanced ^{13}C spectra of surface soil (yellow; sample 1) and the plant on top of the soil (blue). The bottom panel shows the difference of the two spectra, revealing a signature pattern of lignin, aliphatic and polymethylene, as well as matrix polysaccharides. **b,** Carbohydrate region of DNP enhanced ^{13}C-^{13}C refocused J-INADEQUATE spectrum showing signals from cellulose and xylan. Inset picture shows the original plant material characterized here. **c,** Aromatic amino acids resolved from the plant sample, with chemical shifts labeled on the structure. **d**, 2D ^{1}H-^{13}C correlation spectrum measured using 0.1 ms CP resolving key signals of cellulose, xylan, lipid polymers. Lignin methoxyls (-OCH_3 or -OMe) and xylan acetyls (Ac) are also observed, with structures presented. **e**, 2D ^{1}H-^{13}C correlation spectrum measured using 1 ms CP resolving signals of aromatic and carbonyl carbons from proteins and lignin. Dash lines in blue and red annotate the key positions of methoxyl and aromatic protons, respectively. Black dashed line represents the anticipated correlations between lignin aromatic carbons and carbohydrate anomeric protons, which are notably less numerous than the signals observed in the soil.

Strong signals of aromatic amino acid residues have been spotted, which align with the chemical shifts of histidine or tryptophan (**Fig. 2c**). These molecules are uniquely abundant in the plant material and are not present in the soil underneath it, likely due to being vulnerable to rapid microbial degradation. Though the carbohydrates signals are highly consistent with the soil, the aliphatic region shows a dramatically simplified pattern (**Fig. 2d**), with only 3 peaks from the

methoxyl group of lignin, the CH_2 groups likely from the acyl chain of lipids in the membrane or from the cutan or suberin, and the acetyl group that serves as an important modification of matrix polysaccharides, such as xylan. The aromatic region is simpler (**Fig. 2e**). The key carbon sites of both S and G units are still detectable, with these carbons mainly correlating with the methoxyl and aromatic protons and lacking the cross peak with the anomeric protons of carbohydrates at 4.3-4.5 ppm, suggesting substantially reduced interactions between carbohydrates and aromatic polymers.

Despite the conserved structures of individual carbohydrate and lignin components, soil has two unique structural features that are absent in plant materials. First, non-carbohydrate components are highly concentrated, which is likely caused by the faster degradation rate of polysaccharides compared with lignin and polymethylene polymers. Phenols serve as antioxidant during degradation reactions, while polymethylene polymers contain crystalline domains of aliphatic chains, conferring these polymers with high stability[39,40]. This trend was also confirmed by the analysis of another plant sample collected 30 m inland on the same island (**Extended Data Fig. 5**). Secondly, the aromatics and carbohydrates are more tightly packed in the surface soil than in plants. This finding might originate from the faster decay of primary cell walls that only contain cellulose and soft matrix polysaccharides but does not contain lignin, and/or the removal of intra- and extracellular components leading to tighter packing of residual lignocellulosic components.

Mapping carbon composition and packing along depth

The molecular composition of the soil matter changes with the depth. In the quantitative 1D ^{13}C spectra[41], the content of polymethylene carbons, marked by the intensities of two adjacent peaks at 33 and 31 ppm, increased substantially from sample 1 (0-10 cm interval) to sample 2 (40-50 cm interval), as shown in **Fig. 3a**. These two peaks in polymethylene, also observed in many other soil organic matter samples, correspond to crystalline $(CH_2)_n$ chains in all-*trans* conformation (type-a; 33 ppm) and amorphous regions accommodating both *trans* and *gauche* conformations without long-range order (type-b, 31 ppm)[35]. The self-aggregated nature and limited accessibility of polymethylene might have prevented it from being degraded after deposition in the soil. However, when normalized to the aromatic signal, the polymethylene, together with carbohydrates and carbonyls decrease sequentially as one moves deeper in the soil profile (samples 2-7; age range

from 1963AD to 945AD). These spectral observations were quantified through a deconvolution protocol applied to 1D quantitative spectra (**Extended Data Fig. 6**), using the carbon sites resolved from high-resolution 2D dataset. Carbohydrates exhibit a substantial reduction in their proportion, decreasing from 29% in sample 1 to 20% in sample 7, while the content of aromatics are being enriched from 29% to 36% when moving deeper from the surface (**Fig. 3b**).

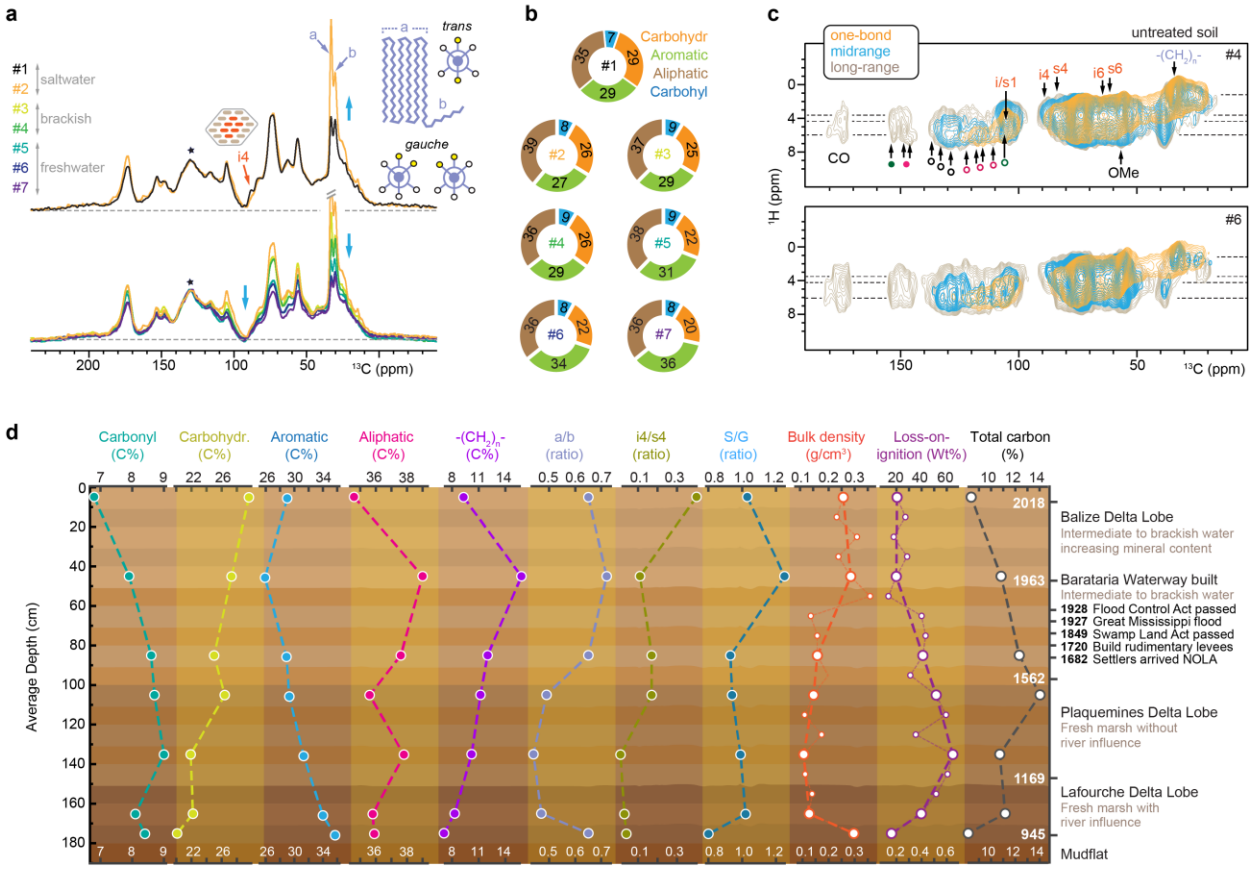

Fig. 3 | Structural changes of SOM in relation to depth. a, Overlay of 1D quantitative ^{13}C spectra of seven soil samples with normalization by the major aromatic peak (asterisk). The top panel compares samples 1 and 2, and the bottom panel includes samples 2-7. The two key peaks (types a and b) of polymethylenes are marked, with an illustration of the crystalline all-*trans* domain and the amorphous domain that include both trans and gauche conformations. Three conformers, *gauche*(+), *gauche*(-), and *trans*, are illustrated, with methylene groups represented as yellow circles and hydrogen atoms as open circles. The wetland condition of each soil sample (saltwater, brackish, or freshwater) are also labeled. **b**, Quantification of the four major carbon types. The details of spectral deconvolution are documented in **Extended Data Fig. 6**, ^{1}H-^{13}C correlation spectra of two untreated soil samples measured with 0.1 ms (yellow), 0.5 ms (light blue), and 1 ms (grey) CP contact times. **d**, molecular and physical evolution of wetland soil over time. The figure depicts a geological timeline through soil depth based on ^{14}C dating results and historic events in the area. Molecular profiling of 7 soil samples reveals the content of major

carbon types. Detailed information differentiates different types of polymethylene carbons, cellulose chains, and monolignol units. Bulk density and loss-on-ignition measurements were also taken on 18 soil samples immediately following collection. A higher bulk density indicates a higher mineral content, while a lower loss-on-ignition % suggests a lower organic matter content.

Regarding the ratio between carbohydrate and aromatic moieties, there is a vertical distribution based on salinity as the wetland transitioned from freshwater, to brackish, to a current day salt marsh environment (**Fig. 3a**)[42]. A similar trend can also be seen regarding the polymethylene-to-aromatics ratio moving from the deeper soil profile to the present-day surface. This finding suggests that, as sea level rises, salinity and resulting shifts in plant species is likely affecting how the sequestered carbon is stored and ultimately degraded in the soil profile.

Native, untreated samples were also investigated using DNP-enhanced 2D ^{1}H-^{13}C correlation experiments (**Fig. 3c**). It is intriguing that the spectral pattern was consistently maintained in the untreated samples 4 and 6 (**Fig. 3c**), and in both HF-treated and untreated materials of sample 1 (**Extended Fig. 7** and **Fig. 1g**); therefore, HF did not perturb the native structure of the SOC core. This similarity is also an indication that at least a significant portion of the lignocellulosic cores were preserved, supported by the observation of internal cellulose, whose carbon 4 (i4) shows a major decline starting from sample 2 (**Fig. 3a**) but still exhibits some weak signals in samples 4 and 6 (**Fig. 3c**). While most cellulose was decomposed rapidly in the surface layers, a fraction of these crystalline cores were preserved for centuries in this wetland soil.

Moreover, the close spatial proximities between aromatics and carbohydrates observed in samples 4 and 6 (**Fig. 3c**) resemble those identified in the surface soil (**Fig. 1g**). The polymethylene also shows the same self-aggregation features in these deeper samples. Therefore, the decomposition of SOM did not happen homogeneously. Some biopolymeric structural cores, like self-aggregated polymethylene and densely packed lignin-polysaccharide domains, have efficiently withstood microbial degradation and maintained their original structure and physical packing after approximately 500 years (at 100 cm depth) and even up to 1000 years (at 180 cm depth). This preservation has been maintained despite the presence of microbial extracellular enzymes present throughout the profile[43].

Natural and anthropogenic influences on carbon speciation over a millennium

The observed nondirectional changes of molecular composition and structure (**Fig. 3d**) are not expected based on conventional soil aging and humification or the activity of microbial communities at depth. As tracked by the ^{14}C dating, the soil material collected across the ~2-m depth covers a geological timeline of 11 centuries[43,44]; therefore, the interplays of the delta lobes and water salinity in the Barataria Bay should also play a key role. The Mississippi River watershed is the dominant surface hydrologic feature in North America, which collects runoff from 40% of the continental US between the Rocky Mountain region to the Appalachian Mountains[42]. River deltas are dynamic systems with continually shifting lobe formation and abandonment over time[42]. Therefore, these environmental shifts, over time, can influence the physical and chemical characteristics of the accreted carbon pool based on hydrodynamics and salinity. One anthropogenic driver has been the construction of river levees over the past century, essentially separating the coastal basins from the river, preventing the historical freshwater and sediment-subsidies from occurring[45].

The continuing decrease of loss-on-ignition (LOI; see Online Methods) and total carbon (TC) and the gradual increase of bulk density (BD) from 1 m depth to the surface of the soil is due to marsh fragmentation (**Fig. 3d**; **Supplementary Methods**). As the continuous marsh platform begins to erode from all edges, the interior of the marsh becomes closer to the shoreline. Consequently, fine-grained sediments present in the bay are transported into the marsh during storm events.[46,47]. The soil at 40 cm depth formed under hypersaline condition also shows the most unique chemical characteristics that violate the trends on the molecular level. It shows the highest content of aliphatics and polymethylene, and the polymethylene has a unique structure that is rich in the carbon site resonating at 34 ppm (named type-a polymethylene; the crystalline domain in *all-trans* conformation). The lignin amount is low but contains a high level of S-monolignols with a high degree of methoxy substitutions. Cellulose crystallinity also becomes low: only 10% of glucan chains are now in a crystalline interior environment, while the remaining majority are disordered.

Paradigm of wetland POM preservation and carbon sequestration

It is imperative to understand the connection between the chemical stability of wetland SOC and its carbon structure, given wetlands' crucial role in global carbon stocks and their ability to

sequester more carbon per unit area compared to other soil types[1,6]. It is also crucial to differentiate between molecular and carbon speciation, microbial transformation, and preservation[17,18] when considering SOC persistence as sea level continues to rise globally[8,12]. In this pursuit, ^{13}C ssNMR spectroscopy[48-50], along with the sensitivity enhancement yielded by DNP[51,52], has been introduced to minimize the biases introduced by the extraction, solubilization, and relaxation present in liquid state NMR (**Supplementary Discussion**), while leveraging the detailed molecular view NMR spectroscopy allows, especially multidimensional techniques. This technique has allowed new insights into SOC sequestration and the importance of preservation for organic rich and POM-dominated blue carbon systems.

This study reveals robust preservation of the polymeric assembly in the top 10 cm of soil echoing the core structure of plant parent materials, evident in the comparable interior and surface cellulose signals, the preservation of multiple forms of cellulose, xylan conformers, and both the S and G monolignols in lignin (**Fig. 1c, e, f**). This result can be attributed to the tight packing of some lignin and carbohydrate components, which could be induced by the decay of bulky cell wall cellulose and soft matrix polysaccharides, as evidenced by lower content of these moieties within the whole soil (**Fig. 2a**). Further evidence for decay taking place in parallel with preservation is the absence of aromatic amino acids within the SOM (**Fig. 2c**). This new insight allows for a refocusing on the concept of molecular preservation in the form of the conservation of the structural core of parent biopolymers, i.e., recalcitrance, as an important component of carbon storage, especially for high organic matter soil systems, such as we find in wetlands, and counters the concept that free POM, as a whole, is a less than stable form of carbon[53,54].

The preservation of recalcitrant lignocellulosic domains in soil POM involves maintaining both the molecular structure and supramolecular assembly of participating biopolymers (**Fig. 3c**). This concurs with the biomolecular transformation of more-accessible molecules on the millennium timescale. The rapid decay of carbohydrates can be explained by their natural preferential utilization by microbes over other molecules, such as aromatic compounds, as both an energy and a nutrient source under the anaerobic soil conditions[53]. The better preservation of aromatics over polymethylene is likely related to the reduced soil conditions. While soil microbes can produce extracellular compounds such as phenol oxidase, these metalloenzyme require oxygen to oxidize

phenol compounds. Hence, in the anaerobic wetland soil profile, these compounds are stable[11]. Additionally, it has been found that high phenolic compounds strongly inhibit hydrolases further muting microbial decomposition of SOM[55], thus we posit that to a limited extent additional aromatic moieties are synthesized by biotic/abiotic processing of the loosely associated lignocellulose[56-58].

The dynamics of deltaic systems on C sequestration were revealed through quantitative ^{13}C NMR data, with major transformations found to occur within the SOC pool over a millennium (**Fig. 3a, d**). The first important takeaway is that the conditions of the wetland under which the SOC is initially preserved play a major role in the decomposition of the SOC pool. This is evidenced by an increased preservation of the carbohydrate when the wetland transitioned from freshwater, to brackish, to a saltwater-dominated wetland (**Fig. 3a**); the same general trend can also be seen regarding polymethylene. The relative proportion of preservation only changed with time with the change in the depositional environment, highlighting the environmental controls on plant species as the dominant factor. The initial transition from a freshwater to brackish water wetland was due to geological influences in the form of lobe transition (Lafourche to Plaquemine lobe and Plaquemine to Balize lobe, respectively), while the transition from a brackish water to a salt marsh was influenced by both a geological lobe relocation and levee construction, starving the wetlands of freshwater and sediment inputs[42].

Conclusions and Perspectives

On aggregate, SOC sequestration in the studied coastal wetland is a combination of molecular—including biomolecular—preservation, recalcitrant carbon, and carbon stabilization through dynamic carbon speciation (biological carbon turnover). The hydrogeomorphic setting changed over the 1000 years during which this sequestration has taken place, transitioning from an active freshwater delta to an abandoned freshwater delta lobe, then to a brackish and, eventually, a salt marsh system, as sea level has continued to rise. Despite these drastic surface changes, preservation, via tighter packing, of parent biopolymers has been consistent over time. A new framework of terminology can be derived, in which preservation can be viewed as molecular preservation and sequestration can be viewed as carbon storage regardless of speciation, with preservation being a subcategory of sequestration. This study provides strong evidence for giving

equal weight to POM, just as what has been done for MAOM in regard to global SOC management[19], with POM being the major focus for organic soils, such as wetlands which contain ~1/3 of the planet's SOC. Recalcitrance should also be a major part of the focus within the preservation of high organic soil, especially as this preserved SOC becomes quickly processed and converted to greenhouse gases when exposed to highly oxygenated water due to erosion[12,13,59]. Therefore, POM and molecular recalcitrance, including biopolymeric structures, are important and may become the main drivers in SOC sequestration for about 1/3 or more of the planet's soil organic carbon pool.

Methods

Collection of soil material. Soil cores (2 m in length) were extracted with a polycarbonate core tube from a brackish *Spartina alterniflora*-dominated island in Barataria Bay, Louisiana, USA (GPS coordinates: 29.44358, -89.899722). Two cores were extracted at different distances (1 m and 2 m, respectively) from the shoreline of the island (**Extended Fig. 1d**). The extracted materials were divided into 10 cm sections based on depth. The samples were stored on ice during transportation and then kept at 4 °C for storage until analyzed.

Hydrofluoric acid treatment. Visible plant matter was removed from the dried soil samples. Each sample was ground with a mortar and pestle set until the material can pass through a 125 μm sieve. Around 600 mg of ground material was transferred into a 15 mL centrifuge tube, and 10 mL of 2% HF solution was added. The tube was capped and turned end-over-end in a rotary mixer throughout for 9 different time intervals in the following sequence: five 1 h intervals then a 16 h interval followed by two 24 intervals and a finally 72 h interval. In between these intervals, the tubes were placed into a benchtop centrifuge and spun at 2000 rpm for 20 min at room temperature. After centrifugation, the 2% HF solution was decanted and replaced with freshly prepared 2% HF solution. The soil samples were then vacuum filtered with 18 MΩ water for three times to remove the excess HF and freeze-dried for 24 h. This protocol was modified from a previously reported method[26]. Comparison of soil materials before and after HF treatment is shown in **Fig. 1a** and **Extended Data Fig. 8a**.

Solid-state NMR Spectroscopy. For each soil sample, 95-105 mg of HF-treated material were packed into a 4-mm zirconium rotor and measured on a Bruker Avance 400 MHz (9.4 Tesla) NMR spectrometer. All experiments were conducted using a 4 mm probe under 14 kHz MAS at 298 K. 1D quantitative spectra were measured using the MultiCP pulse sequence[41], with 11 CP blocks applied. Each CP block used 1.1 ms contact time, with a delay of 0.6 s between blocks. The acquisition time was set to 25 ms, and the recycle delay was 1 s. For each sample, 16,384 scans were recorded within 35 h. The field strengths of the radiofrequency pulses were 71.4 kHz for both ^{13}C and ^{1}H hard pulses, and 62.5 kHz for ^{1}H decoupling. The ^{13}C chemical shifts were externally referenced to the tetramethylsilane (TMS) scale by calibrating the adamantane CH_2 peak to 38.48 ppm. In this work, all ssNMR and DNP spectra were collected using the software Topspin 4.0 and analyzed in Topspin 4.1 version. Graphs were plotted using Origin Pro 2019b software and Adobe Illustrator CC Cs6 V16.0.0.

To analyze the content of different carbon pools, deconvolution was performed on the 1D quantitative MultiCP ^{13}C spectra using DMfit[60] (20200306 version) following the positions of the peaks resolved from 2D DNP spectra, as detailed in **Extended Data Fig. 6** and **Supplementary Table 1**. This allowed us to convert peak intensities into carbon percentages for different structural motifs including carbohydrates, aromatic, carbonyl, and aliphatic components, as well as the ratios of different carbon sites within each category (**Supplementary Table 2**).

1D rotor-synchronized non-quaternary suppression (NQS) spectra were collected under 14 kHz to identify quaternary carbons[61]. Signals from the protonated carbons were dephased using two delays (30 μs × 2) without heteronuclear decoupling. The CP contact time was 2 ms. The acquisition time and the recycle delay was set to 41 ms and 2 s, respectively. In addition, 1D conventional ^{13}C CP spectra were collected to compare with NQS spectra, with identical experimental parameters. The NQS and CP spectra are shown in **Extended Data Fig. 3.**

Preparation of soil and plant samples for MAS-DNP. A stock solution, which is often referred as the DNP juice was prepared using a mixture of D_2O and H_2O (90:10 Vol%) and 10 mM AsymPolPOK biradical (Catalogue# C015P01, CortecNet)[62]. Another two stock solutions were also prepared with the same radical concentration but using different solvents of d_6-

DMSO/D_2O/H_2O (10/80/10 Vol%) and d_6-DMSO/H_2O (90/10 Vol%). The D_2O (Catalogue# DLM-4DR-PK) and d_6-DMSO (Catalogue# DLM-10TC-PK) were from Cambridge Isotope Laboratories. The details parameters of DNP juice composition used for each sample and the setup parameters of all experiments were listed in **Supplementary Table 3**.

The stock solutions were mixed with three types of materials, including HF-treated and non-treated soil as well as plant materials. Around 50 mg of HF-treated soil material was impregnated in 150 μL of the stock solution and vortexed briefly. The mixture was ground mildly for 20 min using a mortar and pestle to allow the radicals to penetrate the porous components of the soil. 30 mg of the final material were then packed into a 3.2 mm sapphire rotor for measurement. For comparison, the two plant samples (*Spartina alterniflora*) collected from the edge of the island (on top of the soil extraction site) and 30 m inland were also processed for MAS-DNP measurement. Around 30 mg of each plant sample was subjected to the same protocol described above to mix with 10 mM AsymPolPOK. For nontreated soil samples, the protocol was modified regarding the concentration of the bi-radical, which has increased to 30 mM to gain more enhancement. The DNP enhancements and Electron paramagnetic resonance (EPR) spectra (EMX Nano benchtop EPR) measured on the plant and soil samples were shown in **Extended Data Fig. 4** and **8**. The EPR spectra were plotted by MATLAB R2020a with a toolbox Easyspin (6.0.0). The evaluation of the inhomogeneity was explained in **Supplementary Methods**.

2D $^{13}C/^{1}H$-^{13}C correlation experiments enabled by MAS-DNP. In unlabeled samples, the natural-abundance of ^{13}C isotope is very low (1.1%), and the probability of observing connectivity between two carbon-13 nuclei in a 2D ^{13}C-^{13}C correlation spectrum is inhibitory (0.01%). To obtain sufficient sensitivity for measuring 2D correlation experiments[51], the soil and plant samples were measured on a Bruker 600 MHz/395 GHz MAS-DNP system at National High Magnetic Field Laboratory, with the microwave irradiation power set to 12 W. The sample temperature was 104 K and 100 K when the microwave was on and off, respectively. The DNP buildup time was 1.3-4.5 s for all the MAS-DNP samples, including the HF-treated and untreated soil samples as well as the plant materials collected 30 m inland and at the edge of the island. Recycle delays were typically set to be 1.3-fold of the DNP buildup time constant for each sample. 1D ^{13}C CP experiments were measured with and without microwave irradiation under 8 kHz for soil and 10.5

kHz for plant samples, with the CP contact time set to 1 ms. The experimental parameters for all 1D and 2D NMR and MAS-DNP experiments are documented in **Supplementary Table 3**.

2D ^{1}H-^{13}C HETCOR experiments were carried out under 8 kHz or 10.5 kHz MAS frequencies. ^{1}H-^{1}H homonuclear decoupling was achieved using either Phase-Modulated Lee–Goldburg (PMLG)[63] or Frequency-Switched Lee-Goldberg (FSLG) sequence[64] with a ^{1}H transverse field strength of 100 kHz, corresponding to an effective field strength of 122 kHz. To vary the range of detection between the proton and carbon sites, ^{1}H magnetization was transferred to ^{13}C using a Hartmann-Hahn (HH) CP block with a variable length, with 0.1 ms for primarily one-bond correlations, 0.5 ms for intermediate range of correlations, and 1.0 ms for long range correlations.

2D ^{13}C-^{13}C correlation experiments were carried out using the refocused INADEQUATE scheme[65]. The experiment was dipolar-based, using the broadband dipolar recoupling SPC5 sequence[66]. The MAS frequencies were 10.5 kHz for the HF-treated soil sample 1 and inland plants, and changed to 8 kHz for the plant samples collected at the island edge. For the direct dimension (ω2), the acquisition time was 17 ms for all soil and plant samples. The acquisition time of the indirect dimension (ω1) was 2.7 ms and 1.7 ms for soil and plants, respectively. The indirect dimensions of the spectra were set to 200 ppm (50 - 250 ppm) to effectively cover the double-quantum chemical shifts of carbohydrate and aromatic polymers. For each sample, 100 increments were collected for the indirect dimension. 320 scans were collected for the soil sample in 16 h, and 160 scans were collected for each of the two plant samples, with experimental time of 13 h and 23 h for the plants on the edge and inland, respectively. To rapidly identify the key carbohydrate components in soil, a probability map was built by extracting 412 datasets of plant carbohydrates from the Complex Carbohydrate Magnetic Resonance Database[36] following a recently reported protocol[67]. All ^{13}C and ^{1}H chemical shifts of identified polymers are documented in **Supplementary Table 4**.

^{14}C dating. Prior to ^{14}C dating, the soil sample was pretreated with an acid/alkali/acid solution to avoid potential effect of the secondary carbon components (roots, bacteria) on the determined age of the sample[43,44]. The decayed plants in the soil were used for ^{14}C dating, which was calibrated to radiocarbon age (years Before Present, yBP) and calendar years (cal AD). The analysis was

performed using BetaCal 3.21, INTCAL13 database, and high probability density range method (HPD). The dataset is summarized in **Supplementary Table 5**.

Bulk density (BD) and loss-on-ignition (LOI). The BD was determined by drying the soil at 60 °C for 24 h in a muffle furnace and then calculated as oven-dry wight per unit volume at field moisture capacity.[9] To determine the LOI, the dried material was ground with a mortar and pestle, and placed into a muffle furnace at 550 °C for 4 h. The mass difference before and after the combustion was divided by the original dry mass to get the percentage value of LOI ratio[13], which represents the relative fraction of organic matter in the sample. The results of these bulk property measurements were detailed in **Supplementary Methods**.

Total carbon percentage. The dried sample was ground using a mortar and pestle and sieved with 125 μm sieve to ensure equal particle size. 10 mg of soil were weighed into ceramic crucibles, which were placed into a total organic carbon analyzer (Shimadzu TOC SSM-5000A) to analyze the content of total carbon. Information on the physiochemical property is documented in **Supplementary Table 5**.

Data Availability

The original datasets of 51 ssNMR spectra collected on soil and plant materials are available in the public repository Zenodo: https://doi.org/10.5281/zenodo.10070388. All relevant data that support the findings of this study are available within the article, Extended Data Figures, and Supplementary Information.

Extended Figures

Extended Figures 1-8

Supplementary Information

Supplementary Methods, Supplementary Discussion, Supplementary Tables 1-5, and Supplementary References.

Acknowledgment

This research was supported by the U.S. Department of Energy under the grant no. DE-SC0021210 to T.W. and the National Science Foundation Chemical Oceanography grants OCE-1636052 and OCE-2054935 to J.R.W. and R.L.C. The National High Magnetic Field Laboratory is supported by the National Science Foundation through NSF/DMR-1644779 and DMR-2128556 and the State of Florida. The MAS-DNP system at NHMFL is funded in part by NIH P41 GM122698 and NIH RM1-GM148766. The authors thank Dr. Alex Kirui for initial data analysis, and M.P. Hayes and Benjamin Haywood for assistance with sample collection and bulk property measurements.

Competing Interest

The authors declare no competing interest.

Author Contributions

W.Z., A.K. F.S. and F. M.-V. collected the MAS-DNP data. E.C.T. collected the room-temperature NMR data. W.Z., D.D., A.K. and E.C.T. analyzed the data. J.R.W. collected the soil samples and conducted the chemical characterization, R.C. and T.W. supervised the project. All coauthors contributed to the writing of the manuscript.

References

1. Nahlik, A.M. & Fennessy, M.S. Carbon Storage in US Wetlands. *Nat. Commun.* **7**, 13835 (2016).
2. Beillouin, D. et al. A global meta-analysis of soil organic carbon in the Anthropocene. *Nat. Commun.* **14**, 3700 (2023).
3. Lal, R. Soil Carbon Sequestration Impacts on Global Climate Change and Food Security. *Science* **304**, 1623-1627 (2004).
4. Georgiou, K. et al. Global stocks and capacity of mineral-associated soil organic carbon. *Nat. Commun.* **13**, 3797 (2022).
5. Ruehr, S. et al. Evidence and attribution of the enhanced land carbon sink. *Nat. Rev. Earth Environ.* **4**, 518-534 (2023).
6. Murray, B., Pendleton, L., Jenkins, W. & Sifleet, S. Green Payments for Blue Carbon: Economic Incentives for Protecting Threatened Coastal Habitats (Nicholas Institute for Environmental Policy Solutions, Duke University, Durham, 2011).
7. Spivak, A.C., Sanderman, J., Bowen, J.L., Canuel, E.A. & Hopkinson, C.S. Global-change controls on soil-carbon accumulation and loss in coastal vegetated ecosystems. *Nat. Geosci.* **12**, 685-692 (2019).
8. Wang, F., Lu, X., Sanders, C. & Tang, J. Tidal wetland resilience to sea level rise increases their carbon sequestration capacity in United States. *Nat. Commun.* **10**, 5434 (2019).
9. Duarte, C.M., Losada, I.J., Hendriks, I.E., Mazarrasa, I. & Marbà, N. The role of coastal plant communities for climate change mitigation and adaptation. *Nat. Clim. Chang.* **3**, 961–968 (2013).
10. Poffenbarger, H.J., Needelman, B.A. & Megonigal, J.P. Salinity Influence on Methane Emissions from Tidal Marshes. *Wetlands* **31**, 831–842 (2011).

11. Reddy, K.R., DeLaune, R.D. & Inglett, P.W. *Biogeochemistry of Wetlands: Science and Application*, (CRC Press, Boca Raton, 2008).
12. Haywood, B.J., White, J.R. & Cook, R.L. Investigation of an early season river flood pulse: Carbon cycling in a subtropical estuary. *Sci. Total Environ.* **635**, 867-877 (2018).
13. Haywood, B.J., Hayes, M.P., White, J.R. & Cook, R.L. Potential fate of wetland soil carbon in a deltaic coastal wetland subjected to high relative sea level rise. *Sci. Total Environ.* **711**, 135185 (2020).
14. Pendleton, L. et al. Estimating Global "Blue Carbon" Emissions from Conversion and Degradation of Vegetated Coastal Ecosystems. *PLOS One* **7**, e43542 (2012).
15. Moomaw, W.R. et al. Wetlands In a Changing Climate: Science, Policy and Management. *Wetlands* **38**, 183-205 (2018).
16. Stevenson, F.J. *Humus Chemistry: Genesis, Composition, Reactions*, (John Wiley & Sons, New York, NY, 1994).
17. Schmidt, M.W.I. et al. Persistence of soil organic matter as an ecosystem property. *Nature* **478**, 49-56 (2011).
18. Lehmann, J. & Kleber, M. The Contentious Nature of Soil Organic Matter. *Nature* **528**, 60-68 (2015).
19. Angst, G. et al. Unlocking complex soil systems as carbon sinks: multi-pool management as the key. *Nat. Commun.* **14**, 2967 (2023).
20. Lehmann, J. et al. Persistence of soil organic carbon caused by functional complexity. *Nat. Geosci.* **13**, 529-534 (2020).
21. Kleber, M. et al. Dynamic interactions at the mineral–organic matter interface. *Nat. Rev. Earth Environ.* **2**, 402-421 (2021).
22. Hall, S.J., Ye, C., Weintraub, S.R. & Hockaday, W.C. Molecular trade-offs in soil organic carbon composition at continental scale. *Nat. Geosci.* **13**, 687-692 (2020).
23. Boesch, D.F. et al. Scientific Assessment of Coastal Wetland Loss, Restoration and Management in Louisiana. *J. Coast. Res.* **20**, 1–103 (1994).
24. Jankowski, K.L., Törnqvist, T.E. & Fernandes, A.M. Vulnerability of Louisiana's Coastal Wetlands to Present-Day Rates of Relative Sea-Level Rise. *Nat. Commun.* **8**, 14792 (2017).
25. Schmidt, M.W.I., Knicker, H., Hatcher, P.G. & Kogel-Knabner, I.K. Improvement of ^{13}C and ^{15}N CPMAS NMR Spectroscopy of Bulk Soils, Particle Size Fractions and Organic Material by Treatment with 10% Hydrofluoric Acid. *Eur. J. Soil Sci.* **48**, 319-328 (1997).
26. Skjemstad, J., Clarke, P., Taylor, J., Oades, J. & Newman, R. The Removal of Magnetic Materials from Surface Soils - A Solid State ^{13}C CP/MAS NMR Study. *Soil Res.* **32**, 1215-1229 (1994).
27. Salati, S., Adani, F., Cosentino, C. & Torri, G. Studying Soil Organic Matter Using 13C CP- MAS NMR: The Effect of Soil Chemical Pre-Treatments on Spectra Quality and Representativity. *Chemosphere* **70**, 2092-2098 (2008).
28. Phyo, P., Wang, T., Yang, Y., O'Neill, H. & Hong, M. Direct determination of hydroxymethyl conformations of plant cell wall cellulose using ^{1}H polarization transfer solid-state NMR. *Biomacromolecules* **19**, 1485-1497 (2018).
29. Wang, T., Yang, H., Kubicki, J.D. & Hong, M. Cellulose structural polymorphism in plant primary cell walls investigated by high-field 2D solid-state NMR spectroscopy and density functional theory calculations. *Biomacromolecules* **17**, 2210-2222 (2016).
30. Kang, X. et al. Lignin-polysaccharide interactions in plant secondary cell walls revealed by solid-state NMR. *Nat. Commun.* **10**, 347 (2019).
31. Kirui, A. et al. Carbohydrate-aromatic interface and molecular architecture of lignocellulose. *Nat. Commun.* **13**, 538 (2022).
32. Busse-Wicher, M. et al. The pattern of xylan acetylation suggests xylan may interact with cellulose microfibrils as a twofold helical screw in the secondary plant cell wall of Arabidopsis thaliana *Plant. J.* **79**, 492-506 (2014).

33. Simmons, T.J. et al. Folding of xylan onto cellulose fibrils in plant cell walls revealed by solid-state NMR. *Nat. Commun.* **7**, 13902 (2016).
34. Grantham, N.J. et al. An even pattern of xylan substitution is critical for interaction with cellulose in plant cell walls. *Nat. Plants*, 859-865 (2017).
35. Hu, W.-G., Mao, J., Xing, B. & Schmidt-Rohr, K. Poly(Methylene) Crystallites in Humic Substances Detected by Nuclear Magnetic Resonance. *Environ. Sci. Technol.* **34**, 530-534 (1999).
36. Kang, X. et al. CCMRD: a solid-state NMR database for complex carbohydrates. *J. Biomol. NMR* **74**, 239-245 (2020).
37. Lattao, C., Birdwell, J., Wang, J.J. & Cook, R.L. Studying Organic Matter Molecular Assemblage within a Whole Organic Soil by Nuclear Magnetic Resonance. *J. Environ. Qual.* **37**, 1501-1509 (2008).
38. Yan, J. et al. Composition Selects Different Soil Microbial Structures and in Turn Drives Different Litter Decomposition Pattern and Soil Carbon Sequestration Capability. *Geoderma* **319**, 194-203 (2018).
39. Lovley, D.R., Coates, J.D., Blunt-Harris, E.L., Phillips, E.J. & Woodward, J.C. Humic Substances as Electron Acceptors for Microbial Respiration. *Nature* **382**, 445-448 (1996).
40. Kögel-Knabner, I., de Leeuw, J.W. & Hatcher, P.G. Nature and Distribution of Alkyl Carbon in Forest Soil Profiles: Implications for the Origin and Humification of Aliphatic Biomacromolecules. *Sci. Total Environ.* **117-118**, 175-185 (1992).
41. Johnson, R.L. & Schmidt-Rohr, K. Quantitative solid-state ^{13}C NMR with signal enhancement by multiple cross polarization. *J. Magn. Reson.* **239**, 44-49 (2014).
42. Coleman, J.M., Roberts, H.H. & Stone, G.W. Mississippi River Delta: an Overview. *J. Coast. Res.* **14**, 698-716 (1998).
43. Sapkota, Y. & White, J.R. Long-term fate of rapidly eroding carbon stock soil profiles in coastal wetlands. *Sci. Total Environ.* **753**, 141913 (2021).
44. Sapkota, Y. & White, J.R. Marsh edge erosion and associated carbon dynamics in coastal Louisiana: A proxy for future wetland-dominated coastlines world-wide. *Estuar. Coast. Shelf Sci.* **226**, 106289 (2019).
45. Alexander, J.S., Wilson, R.C. & Green, W.R. A brief history and summary of the effects of river engineering and dams on the Mississippi River system and delta: U.S. Geological Survey Circular 1375. 43 p. (2012).
46. DeLaune, R.D., Nyman, J.A. & Patrick, W.H. Peat Collapse, Ponding and Wetland Loss in a Rapidly Submerging Coastal Marsh. *J. Coast. Res.* **10**, 1021-1030 (1994).
47. Odum, W.E. Comparative Ecology of Tidal Freshwater and Salt Marshes. *Annu. Rev. Ecol. Syst.* **19**, 147-176 (1988).
48. Simpson, A.J., McNally, D.J. & Simpson, M.J. NMR spectroscopy in environmental research: From molecular interactions to global processes. *Prog. Nucl. Magn. Reson. Spectr.* **58**, 97-175 (2011).
49. Mao, J., Cao, X., Olk, D.C., Chu, W. & Schmidt-Rohr, K. Advanced solid-state NMR organic matter. *Prog. Nucl. Magn. Reson. Spectr.* **100**, 17-51 (2017).
50. Cook, R.L. Coupling NMR to NOM. *Anal. Bioanal. Chem.* **378**, 1484-1503 (2004).
51. Marker, K. et al. Welcoming natural isotopic abundance in solid-state NMR: probing π-stacking and supramolecular structure of organic nanoassemblies using DNP. *Chem. Sci.* **8**, 974-987 (2017).
52. Ni, Q.Z. et al. High frequency dynamic nuclear polarization. *Acc. Chem. Res.* **46**, 1933-1941 (2013).
53. Angst, G., Mueller, K.E., Nierop, K.G.J. & Simpson, M.J. Plant- or microbial-derived? A review on the molecular composition of stabilized soil organic matter. *Soil Biol. Biochem.* **156**, 108189 (2021).
54. Lavallee, J.M., Soong, J.L. & Cotrufo, M.F. Conceptualizing soil organic matter into particulate and mineral-associated forms to address global change in the 21st century. *Glob. Change Biol.* **26**, 261-273 (2020).

55. Freeman, C., Ostle, N. & Kang, H. An enzymic 'latch' on a global carbon store. *Nature* **409**, 149 (2001).
56. Gerke, J. Concepts and misconceptions of humic substances as the stable part of soil organic matter: A review. *Agronomy* **2018**, 18258 (2018).
57. Cao, X. & Schmidt-Rohr, K. Abundant Nonprotonated Aromatic and Oxygen-Bonded Carbons Make Humic Substances Distinct from Biopolymers. *Environ. Sci. Technol. Lett.* **5**, 476-480 (2018).
58. De Nobili, M., Bravo, C. & Chen, Y. The spontaneous secondary synthesis of soil organic matter components: A critical examination of the soil continuum model theory. *App. Soil Ecol.* **154**, 103655 (2020).
59. Steinmuller, H.E. et al. Does edge erosion alter coastal wetland soil properties? A multi-method biogeochemical study. *Catena* **187**, 104373 (202).

References for Online Methods

60. Massiot, D. et al. Modelling one and two-dimensional solid-state NMR spectra. *Magn. Reson. Chem.* **40**, 70-76 (2002).
61. Opella, S.J. & Frey, M.H. Selection of nonprotonated carbon resonances in solid-state nuclear magnetic resonance. *J. Am. Chem. Soc.* **101**, 5854-5856 (1979).
62. Mentink-Vigier, F. et al. Computationally Assisted Design of Polarizing Agents for Dynamic Nuclear Polarization Enhanced NMR: The AsymPol Family. *J. Am. Chem. Soc.* **140**, 11013-11019 (2018).
63. Vinogradov, E., Madhu, P.K. & Vega, S. High-resolution proton solid-state NMR spectroscopy by phase-modulated Lee–Goldburg experiment. *Chem. Phys. Lett.* **314**, 443-450 (1999).
64. Bielecki, A., Kolbert, A.C., De Groot, H., Griffin, R.G. & Levitt, M.H. Frequency-Switched Lee—Goldburg Sequences in Solids. *Adv. Magn. Reson.* **14**, 111-124 (1990).
65. Lesage, A., Bardet, M. & Emsley, L. Through-bond carbon-carbon connectivities in disordered solids by NMR. *J. Am. Chem. Soc.* **188**, 10987-10993 (1999).
66. Hohwy, M., Jakobsen, H.J., Eden, M., Levitt, M.H. & Nielsen, N.C. Broadband dipolar recoupling in the nuclear magnetic resonance of rotating solids: A compensated C7 pulse sequence. *J. Chem. Phys.* **108**, 2686-2694 (1998).
67. Zhao, W., Debnath, D., Gautam, I., Fernando, L.D. & Wang, T. Charting the Solid-State NMR Signals of Polysaccharides: A Database-Driven Roadmap. *Magn. Reson. Chem.*, in press (2023). DOI: 10.1002/mrc.5397

Extended Data Figures

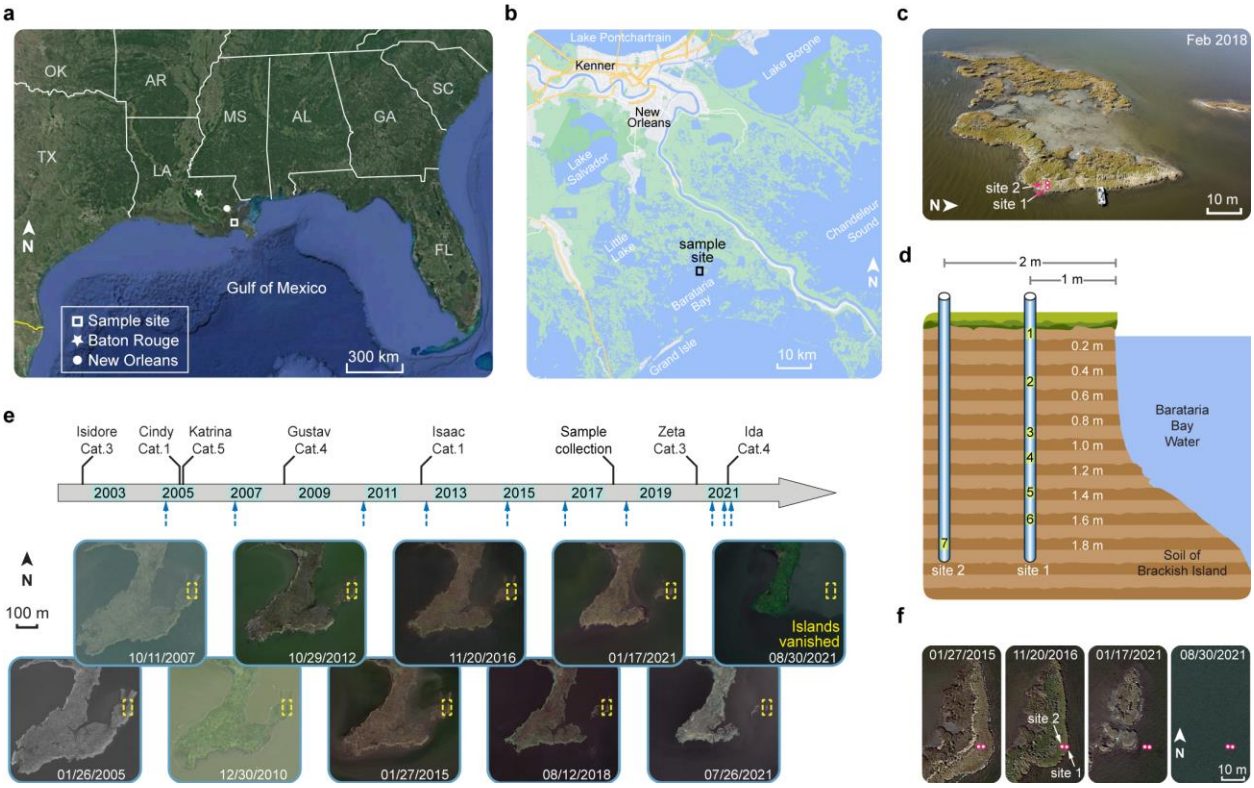

Extended Data Fig. 1 | Wetland soil from a recently vanished brackish island. a, The island is 55 km southeast of New Orleans, and 160 km away from Baton Rouge, the capital city of the state of Louisiana, USA. **b,** Soil materials were collected in February 2018 from a brackish island in Barataria Bay (GPS coordinates: 29°26'36.9"N, 89°53'59.0"W). **c**, Picture of the *Spartina alterniflora*-dominated island with the two sample sites marked. **d,** Location and depth of seven soil samples used for structural characterization. Two poles were used to extract the soil materials, which were divided into 10-cm sections, based on the depth. **e,** Timetable summarizing the landscape change of the island and adjacent lands over two decades. The catastrophic hurricanes that affected this island and the category (Cat.) numbers of these hurricanes are labeled. Blue dashline arrows indicate the ten time points where pictures of the landscape are provided. **f,** Zoom-in view of the dashline boxes in panel (e). Positions of the two sample sites are marked using magenta circles to guide the comparison. The island has been rapidly shrinking, and finally disappeared in 2021.

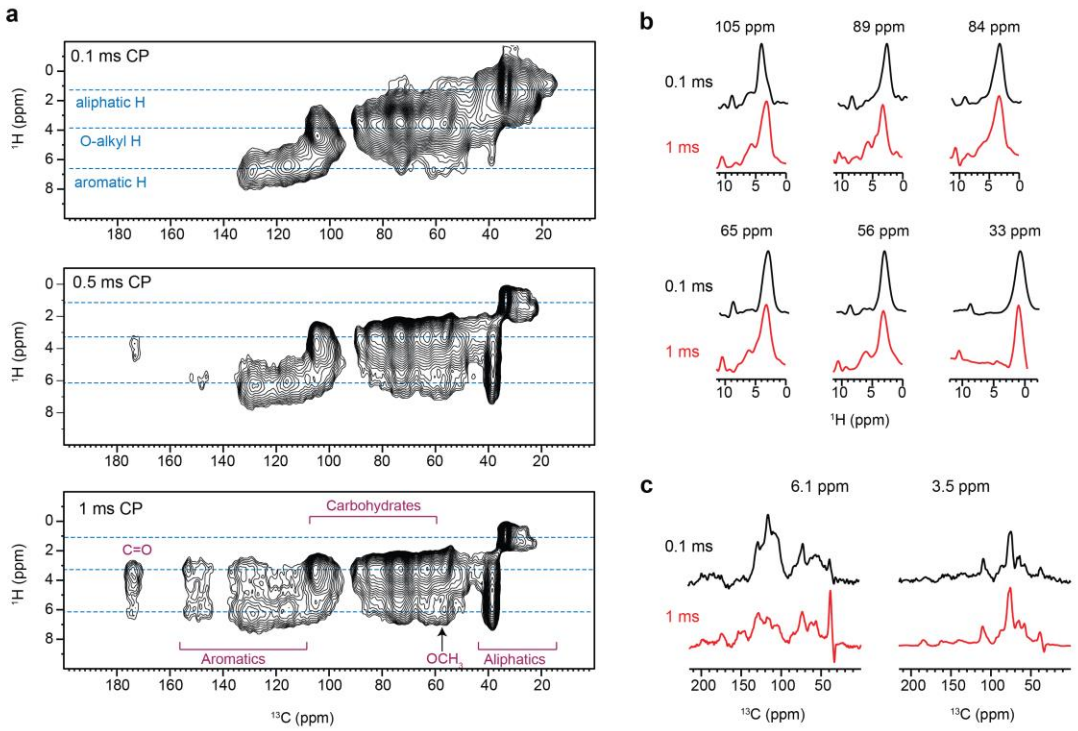

744

745 **Extended Data Fig. 2 | DNP 2D ^{1}H-^{13}C correlation spectra of unlabeled HF treated soil. a,** 2D ^{1}H-^{13}C
746 correlation spectra measured with short (0.1 ms), medium (0.5 ms), and long (1.0 ms) of CP contact times
747 of unlabeled soil sample 1. The blue dash lines show the key proton positions of aliphatics, carbohydrates,
748 and aromatics. The spectrum with 1 ms CP shows intermolecular cross peaks between aromatics and
749 carbohydrates. **b,** Representative ^{1}H cross sections extracted at different carbon sites from the 0.1 ms (black)
750 and 1 ms (red) CP contact times. **c,** Representative ^{13}C cross sections from the 0.1 ms (black) and 1 ms (red)
751 CP contact times. The spectra were measured at 10.5 kHz.
752
753

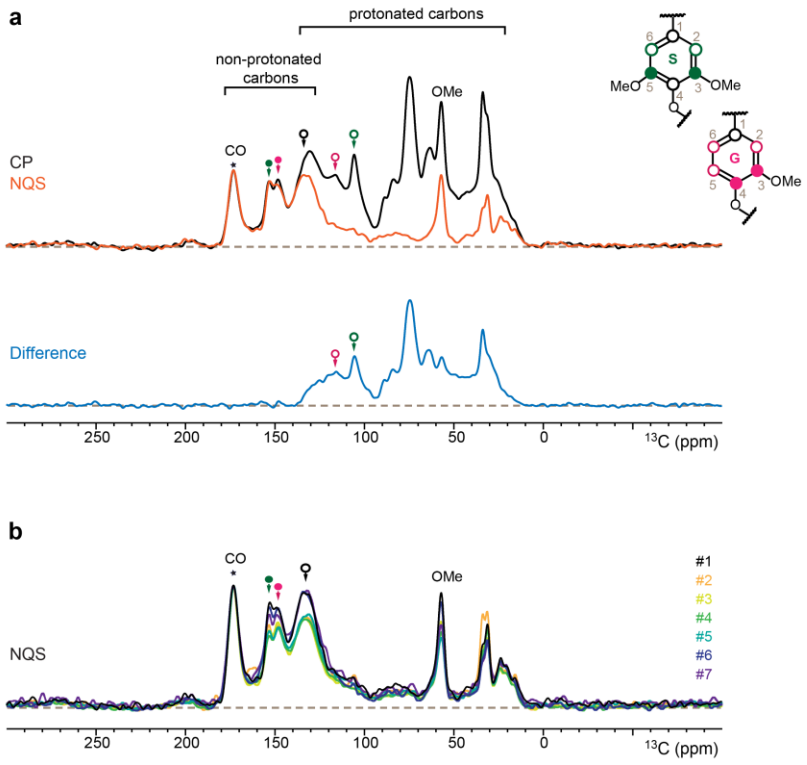

Extended Data Fig. 3 | 1D non-quaternary suppression selectively detecting non-protonated carbons. **a**, Comparison of ^{13}C CP and NQS spectra of the HF treated soil sample #1 at room temperature. The difference spectrum shows only protonated carbons. **b**, Overlay of 1D NQS ^{13}C spectra of seven soil samples. All spectra are normalized by the CO peak (asterisk). QNS spectra mainly shows non-protonated carbons, with methyl carbons as an exception due to their rapid molecular motions.

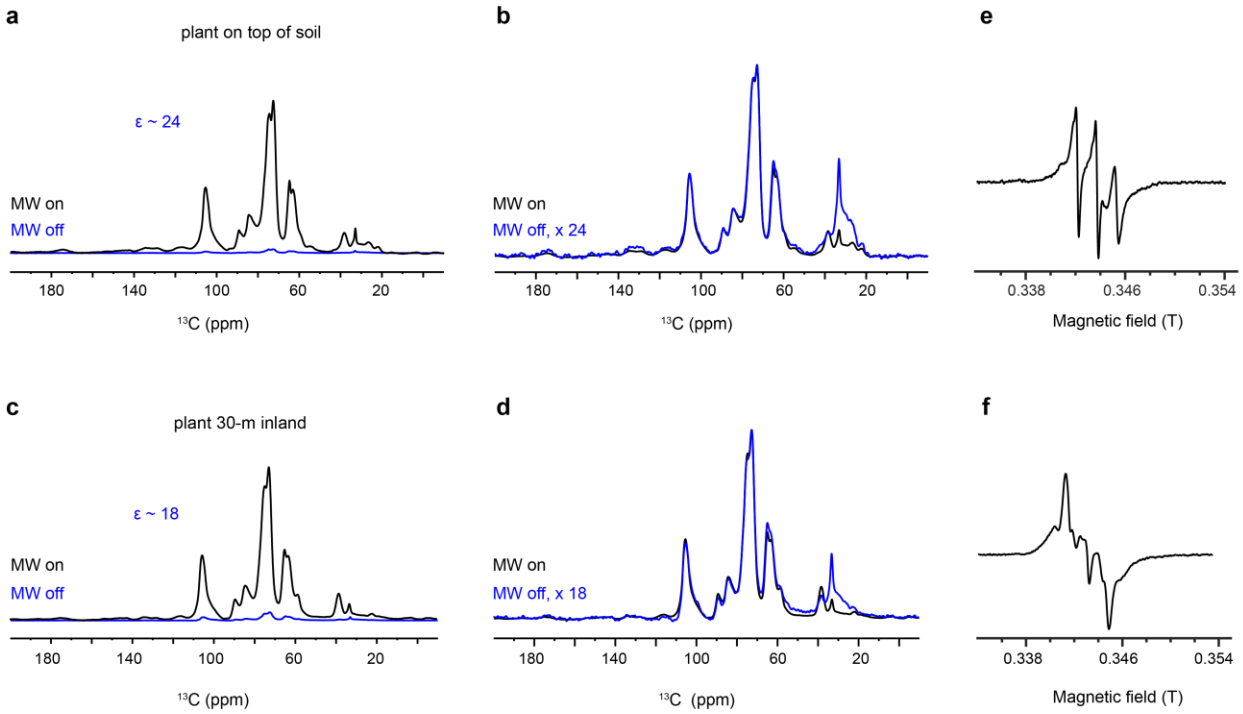

Extended Data Fig. 4 | DNP and EPR spectra of plant samples. a, DNP enhances the sensitivity by 24-fold for the plant on top of soil (on the edge of the island). **b,** Magnification of the microwave (MW) off spectra showed overall consistent pattern with the MW-on spectra, revealing homogeneous polarization by DNP, except for the polymethylene peaks. **c** and **d,** The 30 m inland plant sample also showed 18-fold of DNP enhancement, with homogeneous DNP of carbohydrates and aromatics as shown in panel **e**. **f,** Room temperature EPR spectra of AsymPolPOK (D_2O/H_2O, 90/10 Vol%) at 9.6 GHz for these inland plants.

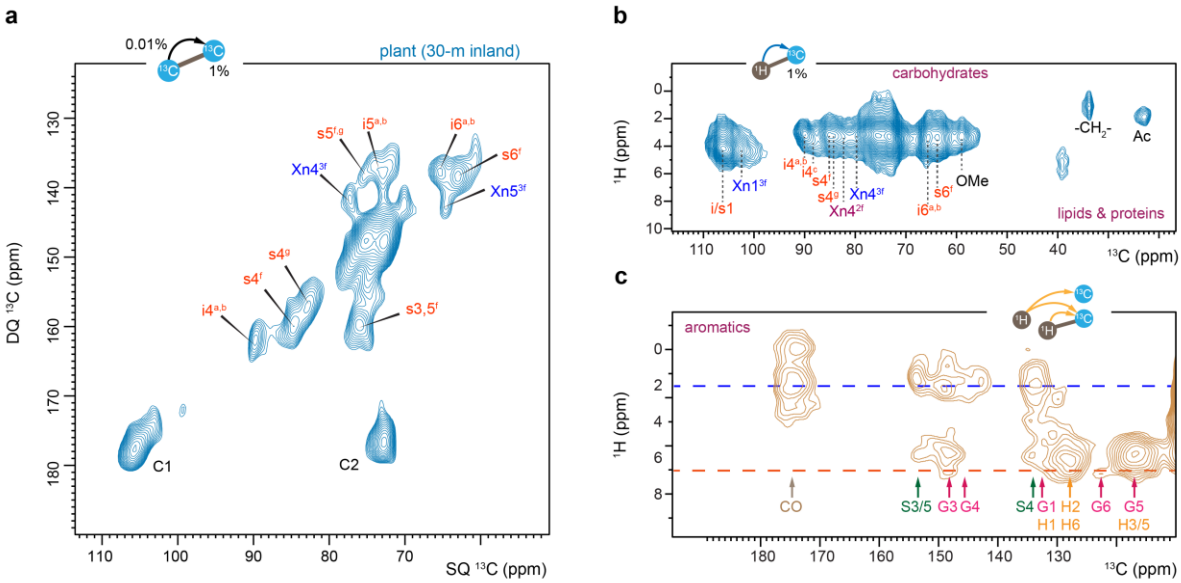

Extended Data Fig. 5 | 2D $^{13}C/^{1}H$-^{13}C spectra of unlabeled plants 30-m inland. a, Carbohydrate region of DNP enhanced ^{13}C-^{13}C refocused INADEQUATE spectrum of unlabeled plant samples collected 30-m inland. Signals are resolved for cellulose and xylan. **b**, 2D Carbohydrate and aliphatic region of 2D ^{1}H-^{13}C HETCOR spectrum of the 30-m inland plant. A short 0.1 ms CP was used to emphasize the one-bond correlations. **c**, The aromatic region collected with long (1 ms) CP contact to show aromatic-aliphatic correlations. No cross peaks were observed with carbohydrates. The spectroscopic features are largely consistent in the plants collected at different locations of the island.

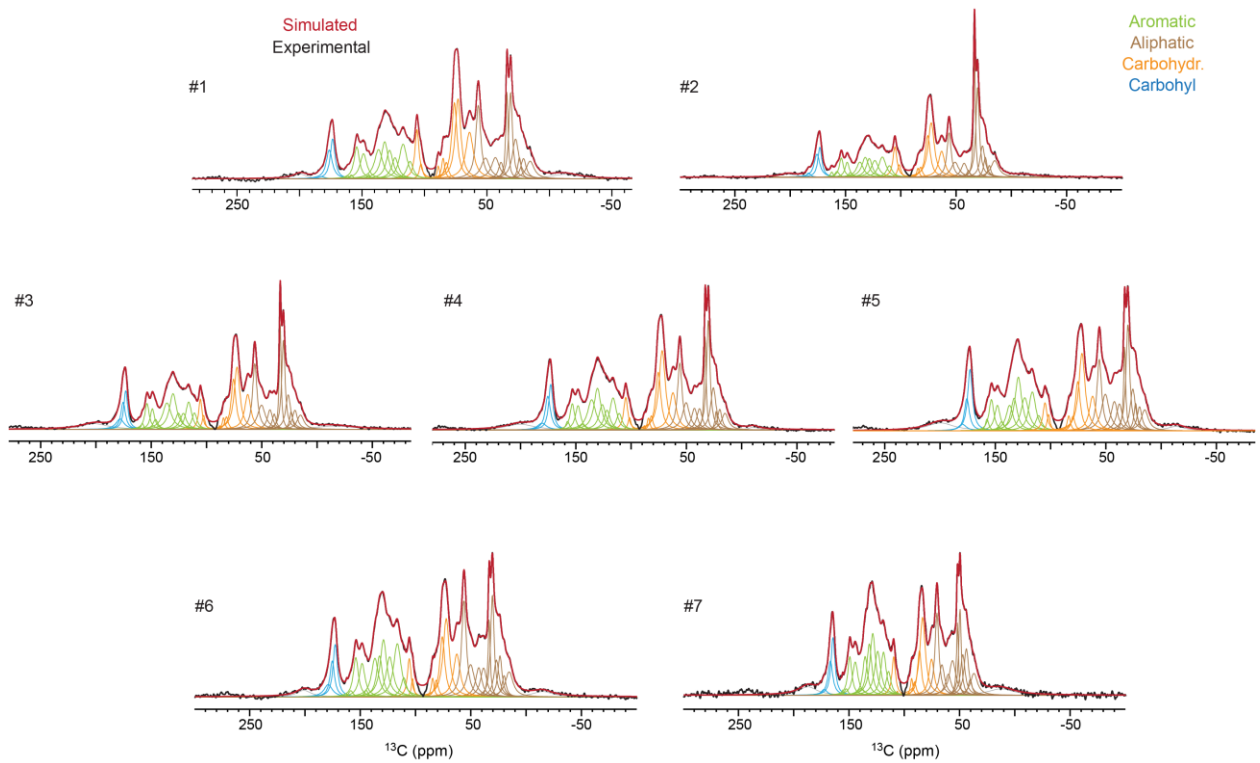

Extended Data Fig. 6 | Spectral deconvolution of quantitative ^{13}C spectra for molecular composition. For each sample, the simulated spectra (dark red) fit the experimentally measured 1D ^{13}C MultiCP spectra (black). Underneath are the individual peaks that contribute to carbohydrate (orange), aliphatic (brown), aromatic (green) and carbonyl sites (blue). The peak list is guided by the resolvable sites obtained from high-resolution 2D data. Information on the deconvolution was documented in **Supplementary Table 1**.

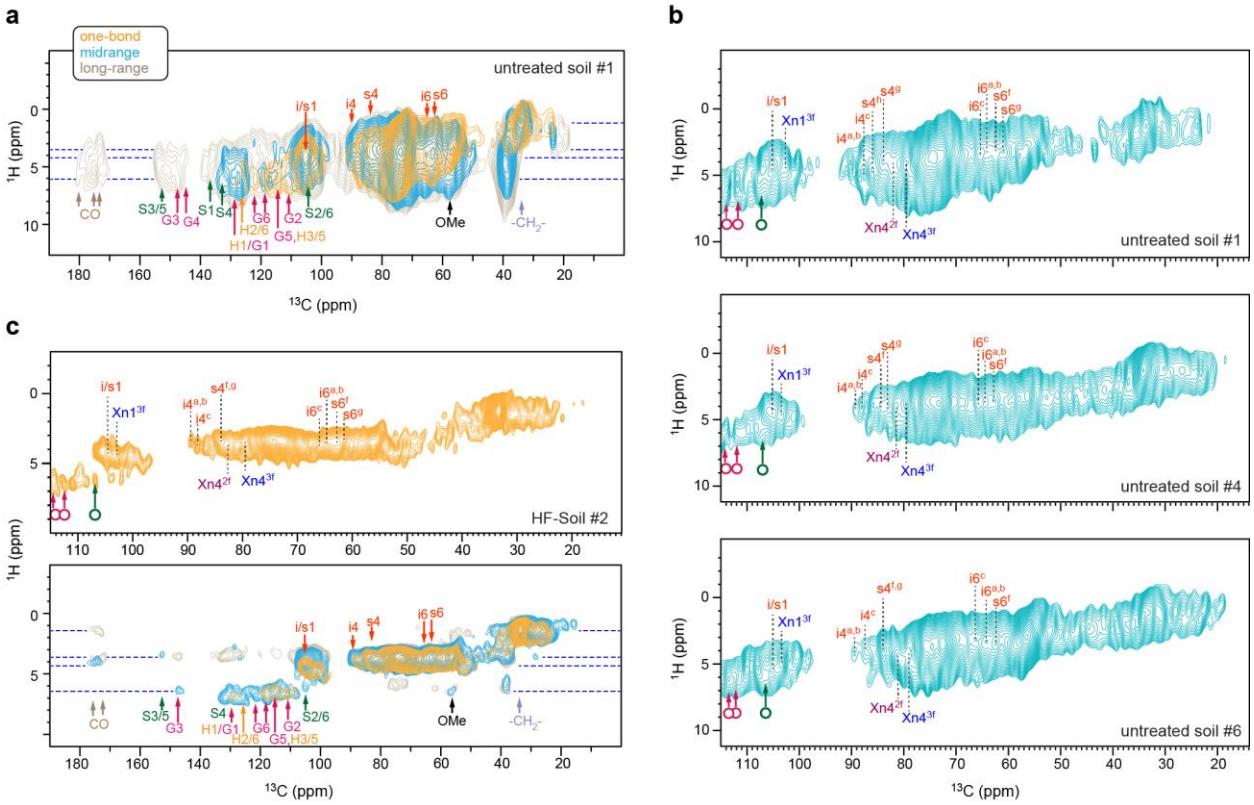

Extended Data Fig. 7 | 2D ^{1}H-^{13}C correlation DNP spectra of untreated soil. a, 2D ^{1}H-^{13}C correlation spectra of untreated soil sample 1 measured with 0.1 ms (yellow), 0.5 ms (blue), and 1 ms (grey) CP contact times. **b,** Zoom-in regions of carbohydrate and aliphatic signals in three untreated soil samples (1, 4, and 6). **c,** Additional 2D ^{1}H-^{13}C spectra of HF-treated soil sample 2. The key signals of carbohydrates and aromatics are observable. Top and bottom panels show the aliphatic/carbohydrate and aromatic signals, respectively.

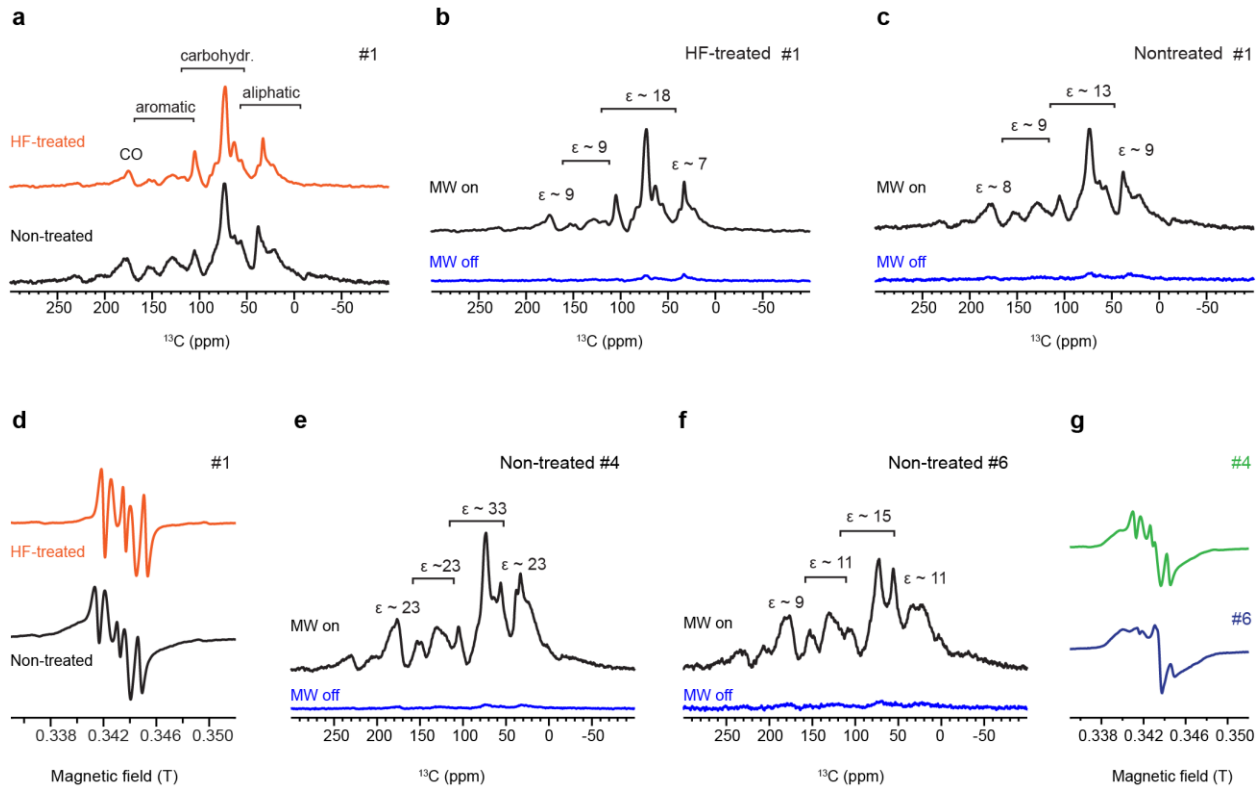

Extended Data Fig. 8 | 1D DNP ^{13}C spectra and EPR of soil samples. a, Comparison of ^{13}C spectra of the HF and non-HF treated materials of soil sample #1 under DNP enhancement. **b**, Comparison of ^{13}C spectra with and without microwave (MW) irradiation collected on HF-treated soil sample 1. The enhancement is 18-fold for carbohydrates, 9-fold for aromatics, 7-fold for CO, 9-fold for most aliphatic carbons, and 7-fold for the polymethylene CH_2 peak. **c,** MW-on and MW-off spectra of non-treated soil sample 1. The enhancement is 13-fold for carbohydrates, 9-fold for aromatics, 8-fold for CO, and 8-fold for most aliphatic carbons, and 9-fold for the polymethylene CH_2 peak. **d**, EPR spectra of soil sample #1 with (top) and without (bottom) HF treatment, hydrated using the d_6-DMSO/D_2O/H_2O matrix. **e,** ^{13}C spectra with and without microwave (MW) irradiation collected on native soil sample #4 without HF treatment, showing enhancement factor of 33-fold for carbohydrate and 23-fold for all other carbon sites. **f,** MW-on and MW-off spectra of untreated soil sample #6, showing enhancement of 15 for carbohydrate and 9-11 for other carbon sites. **g**, EPR spectra of AsymPolPOK at 9.6 GHz for untreated sample #4 (green) and #6 (blue), with a solvent of d_6-DMSO/D_2O (90:10 Vol%).